Robotics and Autonomous Systems 57 (2009) 828–838

Contents lists available at ScienceDirect

Robotics and Autonomous Systems

journal homepage: www.elsevier.com/locate/robot

Hardware design and gait generation of humanoid soccer robot Stepper-3D

H. Dong *, M.G. Zhao, J. Zhang, N.Y. Zhang

Department of Automation, TNList, Tsinghua University, Beijing 100084, PR China

ARTICLE INFO

Article history:
Available online 8 April 2009

Keywords:
Humanoid
Biped locomotion
Virtual slope walking

ABSTRACT

This paper presents the hardware design and gait generation of humanoid soccer robot Stepper-3D. Virtual Slope Walking, inspired by Passive Dynamic Walking, is introduced for gait generation. In Virtual Slope Walking, by actively extending the stance leg and shortening the swing leg, the robot walks on level ground as it walks down a virtual slope. In practical, Virtual Slope Walking is generated by connecting three key frames in the sagittal plane with sinusoids. Aiming for improving the walking stability, the parallel double crank mechanism are adopted in the leg structure. Experimental results show that Stepper-3D achieves a fast forward walking speed of 0.5 m/s and accomplishes omnidirectional walking. Stepper-3D performed fast and stable walking in the RoboCup 2008 Humanoid competitions.

1. Introduction

Recently, significant advances in humanoid robotics concerning walking, hardware and software design have been achieved. Particularly in the RoboCup Humanoid League, where robotics and artificial intelligence research are promoted, designing a soccer robot with fast and stable walking ability is the key point to the ultimate goal of the RoboCup initiative, which is to develop a team of fully autonomous humanoid robot soccer players that shall be able to beat the champion of the most recent World Cup under FIFA official rules by the mid-21st century [1]. Among the current soccer robots in RoboCup Humanoid League, significant progress has been made in the construction of the platform, such as the robots from team NimbRo [2], VisiON NEXTA from team OSAKA [3], Bruno from team Darmstadt Dribblers & Hajime [4], Robo-Erectus from team RoboErectus [5]. All of the above soccer robots are constructed with servo motors regarding a low cost and robust hardware. Equipped with the pocket PC or PC104 as the main computer, these robots exhibit fully autonomous behaviour in the soccer game.

Currently, most biped walking robots are built around trajectory tracking, with the 'Zero Moment Point' (ZMP) criterion [6] to ensure its stability, such as ASIMO [7] with the currently highest speed of 6 km/h. The ZMP is defined to be the point on the ground where the influence of all ground-reaction forces can be replaced by one single force. The ZMP criterion states that when the ZMP is contained within the interior of the support polygon, the robot is dynamically stable [6]. Such an artificial constraint is somewhat too restrictive in that it inherently limits the performance of the gait [8]. The robots are under-achieving in terms of speed, efficiency, disturbance rejection, and natural appearance compared to human walking [9].

The solution to increase the performance is to release the constraints even more, producing a completely different approach, namely Passive Dynamic Walking. McGeer showed that a planar biped may walk down a shallow slope without any control or actuation, presenting human-like natural motions [10]. This approach resulted in highly efficient gaits, but limited versatility that they only walked at one speed for a given slope. The concept of Passive Dynamic Walking has been used as a starting point for designing actuated walkers that are able to walk on level ground [9]. As McGeer stated in [11], there are several options for adding power and control to the passive walking model for level ground walking, such as torque application between legs, torque on the stance leg only, leg length modulation, and impulse application on the trailing leg as it leaves the ground. The delft pneumatic biped Denise [12] has been developed by applying torque at the hip joint. And Meta [13] is developed by applying torque at the ankle joint. The Cornell biped [14] is developed by impulse application on the trailing leg as it leaves the ground with the minimal energy use. The above passive-based powered walkers achieved significant advances in terms of energy efficiency and disturbance rejection ability.

Virtual Slope Walking is a full powered walking inspired by Passive Dynamic Walking. The swing leg is shortened relative to the stance leg prior to the heelstrike, then the effect would be like taking a downhill step, which we named Virtual Slope. Since the swing leg can not be shortened infinitely, after heelstrike, the leg shortened in the previous step will be extended. According to the basic conditions for stable gait, The Virtual Slope Walking gait can be generated by connecting three key frames with simple sinusoids in the sagittal plane. Tested on the Stepper-2D, it is indicated from

* Corresponding author. Tel.: +86 10 62794322; fax: +86 10 62786911.
E-mail address: donghao00@mails.tsinghua.edu.cn (H. Dong).
URL: http://www.au.tsinghua.edu.cn/robotlab/rwg/ (H. Dong).

0921-8890/$ – see front matter © 2009 Elsevier B.V. All rights reserved.
doi:10.1016/j.robot.2009.03.009

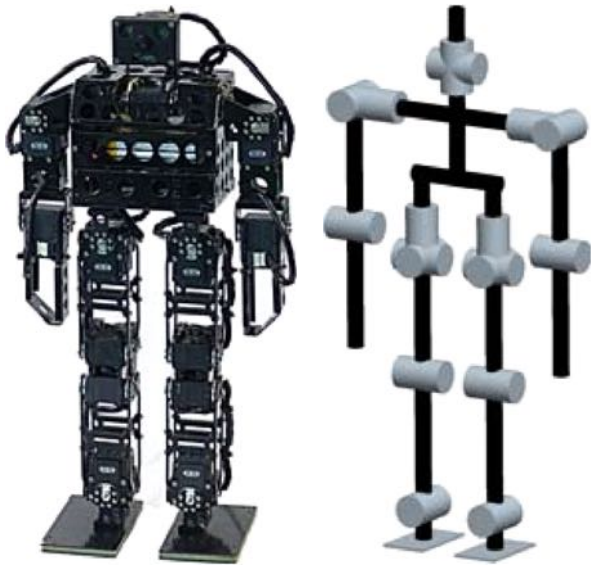

(a) Stepper-3D. (b) Configuration of DOFs.

Fig. 1. A view and configuration of DOFs of Stepper-3D.

the experiment result that Virtual Slope Walking is effective in generating fast and stable walking.

We construct a humanoid soccer robot named Stepper-3D as an application of Virtual Slope Walking in the RoboCup Humanoid competitions. The PDCM is adopted in the leg structure to increase the walking stability. Applying Virtual Slope Walking in the sagittal plane and lateral swing movement in the lateral plane, Stepper-3D achieves fast and stable walking.

The remainder of this paper is organized as follows: In Section 2, the hardware design of our humanoid robot Stepper-3D is presented. In Section 3, Virtual Slope Walking is introduced. In Section 4, we illustrate the gait generation of Virtual Slope Walking. Section 5 presents the experimental results and Section 6 the conclusion and future work.

2. Hardware design of Stepper-3D

2.1. Overview of Stepper-3D

Stepper-3D is the humanoid soccer robot for Tsinghua Hephaestus team to participate in the RoboCup Humanoid League 2008, as shown in Fig. 1(a). The mechanical configuration of Stepper-3D is illustrated in Fig. 1(b). As shown in Fig. 1(b), the upper body is composed of 8 degrees of freedom (DOFs), with orthogonalized axes of pitch and yaw joints in head, orthogonalized axes of pitch and roll joints in shoulder and pitch joints in elbow. Using parallel double crank mechanism (PDCM) in the leg structure, the DOF of lower body is decreased from 12 to 10. The axes of yaw, roll and equivalent pitch joints are orthogonalized and intersect at single points in hip. The pitch joints and roll joints are in the knees and ankles respectively.

Under the competition rules of the RoboCup Humanoid League 2008 [15], Stepper-3D is 476 mm in height and 2.68 Kg in weight. The specifications are shown in Fig. 2. All the joints are actuated by Robotis digital servo motors. Aiming for fast walking, Stepper-3D is designed with the least DOF and as light as possible. Moreover, the movable ranges of the joints of Stepper-3D are designed to perform omnidirectional walking, kicking and recovering from falling down which are all required for humanoid soccer game.

2.2. Leg structure using parallel double crank mechanism

The major design concepts of Stepper-3D are using the PDCM as the leg structure, shown in Fig. 3. Using the PDCM, the feet can be mechanically constrained to be parallel to the ground. Furthermore, compared with the traditional leg structure, the angular cumulative errors caused by the joint motors are eliminated in the PDCM. Additionally, this design saves the two

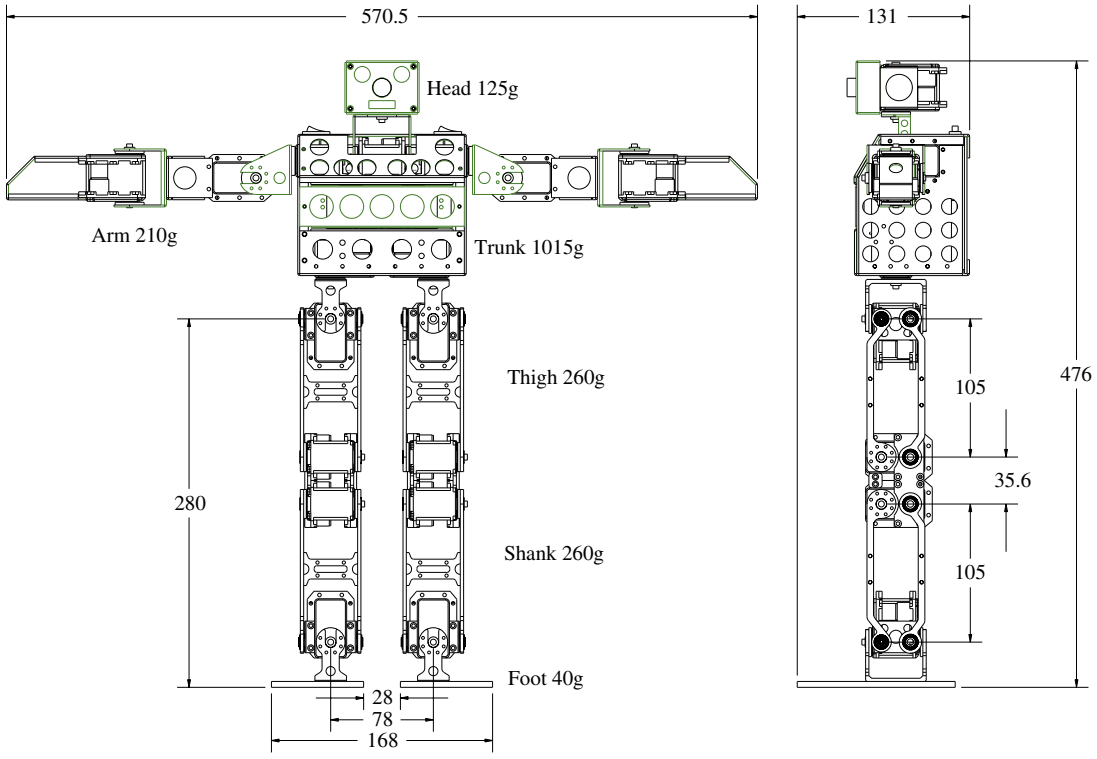

Fig. 2. Specifications of Stepper-3D.

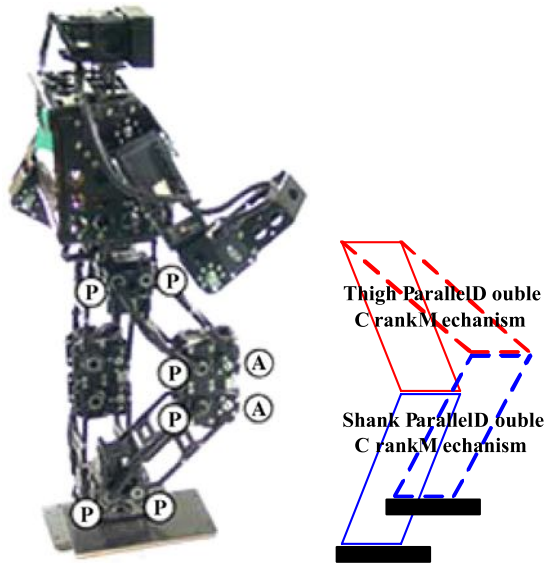

(a) Leg structure of Stepper-3D. (b) Parallel double crank mechanism.

Fig. 3. Stepper-3D with the parallel double crank leg mechanism. (P): Passive rotation axis, (A): Active rotation axis.

ankles' pitch joint and reduces the weight of the legs. Conclusively, the PDCM is the key point in fast walking for lightening the leg weight and eliminating the angular error caused by the ankle pitch motor.

The leg of Stepper-3D is composed of two sets of PDCMs (Fig. 3(b)), forming the thigh and shank respectively. Since this mechanism has only one DOF, any of the four vertexes can be used as the active rotation axis, while the other three rotate passively. On Stepper-3D, the actuators with active rotation axes are placed at the front vertexes of the knee joint (Fig. 3(a)) to simplify the hip structure design, while the hip and ankle vertexes act as passive ones (Fig. 3(a)). The elastic foot is designed by using flexible materials on the bottom of the feet. The table-tennis rubber sheet is added under the elastic carbon fiber sheet which is connected to the ankle roll axis directly. The elastic foot reduces the impact of heelstrike.

2.3. Electronic system

As shown in Fig. 4, Stepper-3D has one PC-104 as the main controller. All motors and sensors of the robot are connected to the main controller by two USB ports and three COM ports. We use the PC-104 as the controller of whole body motion as well as the vision processing and soccer behavior controller.

Specifically, one Logitech QuickCam Pro 5000 CCD camera is selected to be the vision sensor. The USB Wireless card is used for wireless communication. The inclinometer is located in the trunk to detect whether and to which side the robot falls down. Buttons and LEDs, located on the robot back, are set to control and indicate the robot state, and their signals are processed by the MCU communicated with the main controller via a RS-232 serial line at 115200 Baud. The Dynamixel servo motors of head and body are connected in series on a RS-485 Bus respectively. Stepper-3D is powered by high-current Lithium-polymer rechargeable batteries.

3. Principle of Virtual Slope Walking

In Passive Dynamic Walking, a robot walks down a shallow slope without any control or actuation, as shown in Fig. 5. The lost gravitational potential energy while the robot walks downhill is transformed to the walking kinetic energy and gets dissipated at heelstrike [10]. If the slope angle is appropriate, the complementary gravitational potential energy E_s is equal to the dissipation energy E_r at heelstrike, a stable gait can be synthesized [16].

We suppose that the robot leg length can be shortened infinitely and the swing leg can be swung around arbitrarily quickly to the correct pose for the heelstrike. In level ground walking, the swing leg is shortened by a constant ratio during each step. In this

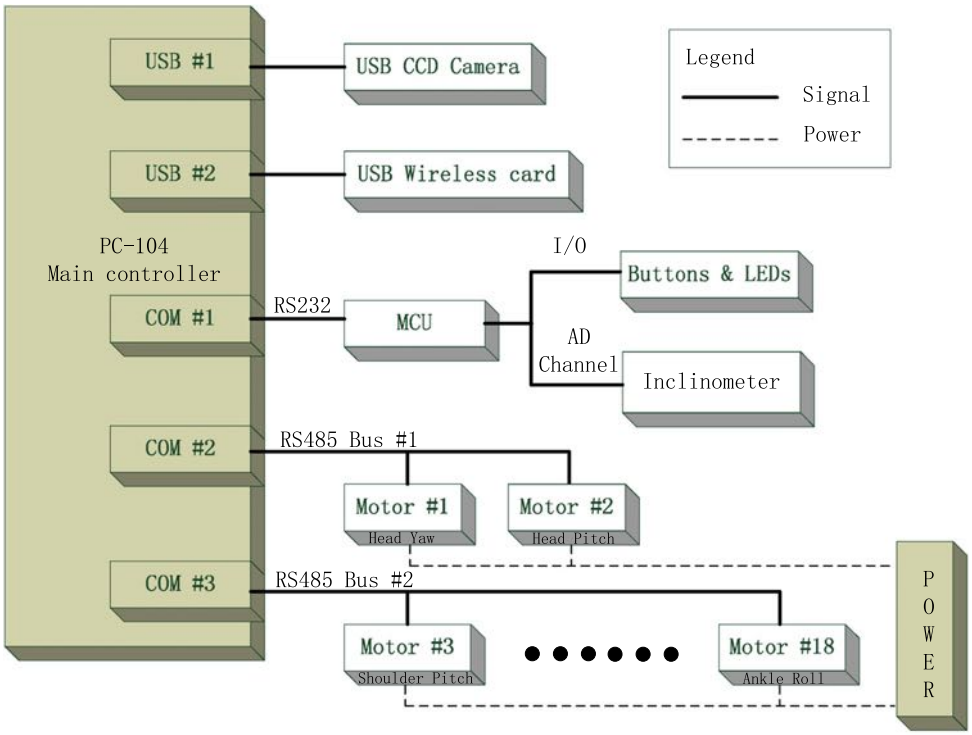

Fig. 4. The electrical system of Stepper-3D.

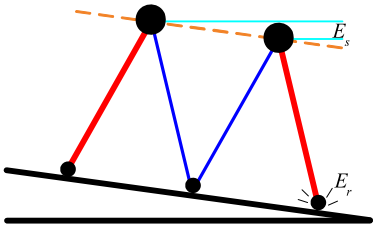

Fig. 5. Passive Dynamic Walking.

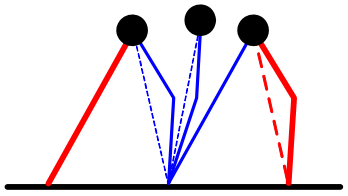

Fig. 7. Realization for Virtual Slope Walking.

way, the center of gravity experiences a virtual slope as shown in Fig. 6(a). Just as in Passive Dynamic Walking, if the angle of the virtual slope is appropriate, the complementary gravitational potential energy E_s by the descending of the center of gravity is equal to the dissipation energy E_r at heelstrike, a stable gait can be achieved continuously. However, in practical walking, the leg length of the robot cannot be shortened infinitely. So after heelstrike, it is required that the stance leg shortened in the previous walking step should be actively extended during the following swing phase with an amount of energy E_c added into the walking system, as shown in Fig. 6(b). If the complementary energy E_c by extending the stance leg is equal to the dissipation energy E_r at heelstrike, a stable gait can be achieved continuously.

For gait generation of Virtual Slope Walking, the stance leg extending can be realized by unbending the knee joint in the swing phase and the swing leg can be shortened by bending the knee joint as shown in Fig. 7. The Virtual Slope Walking gait is then defined as a combined process of actively extending the stance leg (Fig. 7) and actively swinging & shortening the swing leg (Fig. 7).

3.1. Model

The model we studied in the Virtual Slope Walking is shown in Fig. 8, which consists of two massless legs and a point mass body at position (x, y). This model is based on the basic assumption that humans have compact bodies and light legs. And the forces the legs exert on the upper body act through the center of mass, and therefore, applying very little rotational moment on the upper body. The two legs are modeled as a telescoping actuator with a point foot. The leg shortening and extending is realized by bending or unbending the knee joint and following a predefined trajectory. During the swing phase, the stance leg acts as an inverted pendulum with variable length. The stance leg supports compressive force F in the direction of the line joining the point-foot and the point-mass body, as shown in the Fig. 8(a).

Using the *Lagrangian equations*, the two coupled second-order differential equations of motion are given below for the swing phase of the motion.

$$\begin{cases} r\ddot{\theta} + 2\dot{r}\dot{\theta} - g\sin\theta = 0 \\ m\ddot{r} - mr\dot{\theta}^2 + mg\cos\theta = F. \end{cases} \tag{1}$$

The single stance phase ends with a discrete impact when the swing foot hits the ground, which is named heelstrike, as shown in

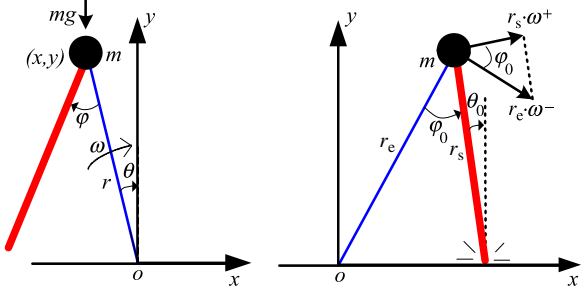

(a) Swing phase. (b) Heelstrike.

Fig. 8. Model in Virtual Slope Walking. m: the mass of the body, r: the length of the stance leg, ω: the angular velocity of the stance leg, θ: the angle of the stance leg with respect to the vertical with the positive sign, φ: the angle between the stance leg and swing leg, g: gravitational acceleration, F: the leg compressive force, r_s: the length of the stance leg right after heelstrike, r_e: the length of the stance leg right before heelstrike, ω^+: the angular velocity of the stance leg right after heelstrike, ω^-: the angular velocity of the stance leg right before heelstrike, φ_0: the angle between the stance leg and swing leg at heelstrike, θ_0: the initial angle of the stance leg at heelstrike.

Fig. 8(b). We assume that the heelstrike behaves as a fully inelastic impact (no slip, no bounce). Also double stance is assumed to occur instantaneously. When the swing leg hits the ground and sticks, the stance leg lifts up. This impact results in an instantaneous change in the velocity of the point mass body. From conservation of angular momentum at the swing foot contact point, we obtain the following transition equation:

$$\omega^+ = \frac{r_e}{r_s}\cos\varphi_0\omega^-. \tag{2}$$

At heelstrike, the angle between the swing leg and stance leg φ_0 and the initial angle of the stance leg θ_0 satisfy the following relationship

$$\varphi_0 = \theta_0 + \arccos\frac{r_s\cos\theta_0}{r_e}. \tag{3}$$

So we obtain the impact equations as follows

$$\begin{cases} \omega^+ = \dfrac{r_e}{r_s}\cos\varphi_0\omega^- \\ \varphi_0 = \theta_0 + \arccos\dfrac{r_s\cos\theta_0}{r_e}. \end{cases} \tag{4}$$

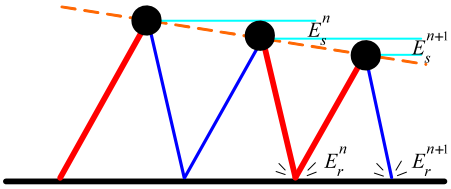

(a) Center of gravity descending through the swing leg shortening.

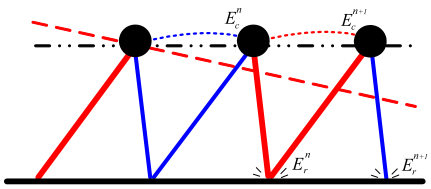

(b) Actively extending the stance leg for energy complement.

Fig. 6. Virtual slope walking.

For the simplification of Virtual Slope Walking, we have three assumptions as follows:

(a) During walking, the single stance foot should be in contact with the ground at all times without slipping, which means there is no flight phase.
(b) The swing leg can be swung around arbitrarily quickly to the correct pose for the heelstrike. Since the swing leg is modeled as having zero mass, this assumption exists distinctly.
(c) The angle between the two legs and the leg length are fixed around heelstrike, which means that $\dot{\varphi_0} = 0, \dot{r_s} = 0, \dot{r_e} = 0$. This assumption is used for the dimension-reduction in the disturbance state space of the system. Once there is a disturbance of the timing of heelstrike, which results in a longer or shorter step period (T) than normal, there is no influence on the variable of φ_0, r_s, r_e.

3.2. Basic conditions for the stable gait

We define a walking step as starting at the beginning of the swing phase or just after the heelstrike of the last walking step, and ending after its heelstrike. With the model and assumptions presented above, two basic conditions have to be satisfied for the existence of stable gait in Virtual Slope Walking:

Condition I. The complementary energy E_c provided by extending the stance leg should be equal to the dissipation energy E_r at heelstrike of step n:

$$E^n{}_c = E^n{}_r. \tag{5}$$

Denoting the angular velocity before and after the heelstrike of step $n-1$ by $\omega^-{}_{n-1}$ and $\omega^+{}_{n-1}$. Let $E^n{}_c$ be the complementary energy of step n and $E^n{}_r$ be the dissipation energy. During the swing phase of step n, we obtain the following equation based on the conservation of energy:

$$E^n{}_c + \frac{1}{2} m {r_s}^2 {\omega^+{}_{n-1}}^2 = \frac{1}{2} m {r_e}^2 {\omega^-{}_n}^2. \tag{6}$$

In the heelstrike transition from step n to step $n+1$, we also obtain:

$$\frac{1}{2} m {r_e}^2 {\omega^-{}_n}^2 = E^n{}_r + \frac{1}{2} m {r_s}^2 {\omega^+{}_n}^2. \tag{7}$$

If the gait is stable, the initial condition of step $n+1$ is exactly equal to that of step n, i.e. $\omega^+{}_n = \omega^+{}_{n-1}$. Therefore, combing Eqs. (6) and (7), the basic Condition I in Eq. (5) is obtained.

Condition II. The timing of extending the stance leg should be after the midpoint in the swing phase.

The gait should be robust to small disturbances if the walking is stable. The stability of the gait is analyzed with the Poincaré mapping, which is a linearized stability analysis of the equilibrium gait. Our Poincaré section is at the start of a step, just after heelstrike. There are two disturbances during the walking: $\Delta\omega_{n-1}$ is the disturbance on the angular velocity of the stance leg just after the heelstrike of step $n-1$; and ΔT_{n-1} is the disturbance of the step period at step $n-1$. $\Delta\omega_{n-1} > 0$ means the stance leg swings faster than normal in step n. $\Delta T_{n-1} > 0$ means the step $n-1$ last longer than usual, resulting in the start of the leg extending at step n postponed accordingly.

The Poincaré mapping method perturbs the two independent initial conditions and monitors the effect on the initial conditions for the subsequent step. Assuming linear behavior, the relation between the original perturbations at step n and the resulting perturbations at step $n+1$ is captured in the Jacobian matrix J, as in:

$$\begin{bmatrix} \Delta\omega_n \\ \Delta T_n \end{bmatrix} = J \begin{bmatrix} \Delta\omega_{n-1} \\ \Delta T_{n-1} \end{bmatrix} = \begin{bmatrix} A & B \\ C & D \end{bmatrix} \begin{bmatrix} \Delta\omega_{n-1} \\ \Delta T_{n-1} \end{bmatrix}. \tag{8}$$

If the eigenvalues of matrix J are all within the unit circle in the complex plane, rendering a small perturbation will decay with time, which will result in a stable gait [17].Therefore, the basic Condition II can be obtained from the eigenvalue equation of matrix J, which represents the relationship between $\Delta\omega$ and ΔT from step n to step $n+1$.

Due to the complexity of the nonlinear, second order, coupled differential motion equations in Eq. (1), we use the following approximation to simplify the equations:

$$\begin{cases} \omega = \overline{\omega} \\ \overline{\omega} = \omega^+ \\ \theta = \theta_0 - \overline{\omega} t \end{cases} \tag{9}$$

where $\overline{\omega} = \frac{\varphi_0}{T}$ is the average angular velocity of the stance leg. Such approximation comes from the simulation result, where the angular velocity of the stance leg approximates to a constant. And the average angular velocity $\overline{\omega}$ appears close to the angular velocity right after heelstrike ω^+.

The complementary energy E_c is the integration of the leg compressive force F over the leg length r provided by extending the stance leg during the swing phase (Fig. 8(a)), as in the following equation:

$$E_c = \int_{r_s}^{r_e} F \mathrm{d}r = \int_{r_s}^{r_e} (mg\cos\theta - m\dot{\theta}^2 r + m\ddot{r}) \mathrm{d}r. \tag{10}$$

With the approximation Eq. (9) and the assumption (c) of $\dot{r_s} = 0, \dot{r_e} = 0$, we obtain the representation of E_c as follows:

$$E_c = \int_{r_s}^{r_e} mg\cos\theta \mathrm{d}r - \frac{1}{2} m\overline{\omega}^2 ({r_e}^2 - {r_s}^2). \tag{11}$$

Denoting the start and the end time of stance leg extending by t_s and t_e, correspondingly, $\theta(t = t_s) = \theta_s$, $\theta(t = t_e) = \theta_e$. Based on the first mean value theorem for integration, since $\cos\theta$ is a continuous function on the closed interval $[\theta_s, \theta_e]$, there exists θ^* in (θ_s, θ_e) such that

$$\int_{r_s}^{r_e} mg\cos\theta \mathrm{d}r = mg\cos\theta^*(r_e - r_s). \tag{12}$$

Therefore, the integrating process of stance leg extending from $\theta = \theta_s$ to $\theta = \theta_e$ is equivalent to extend the stance leg at $\theta = \theta^*$ instantaneously, where $\theta_s < \theta^* < \theta_e$. The complementary energy E_c is then represented as follows

$$E_c = mg\cos\theta^*(r_e - r_s) - \frac{1}{2} m\overline{\omega}^2 ({r_e}^2 - {r_s}^2). \tag{13}$$

Letting $\Delta\omega_{n-1} \to 0$ and $\Delta\theta^*{}_n \to 0$ be the disturbance of ω and θ^* in step n, the full differential equation of Eq. (13) is as follows:

$$\Delta E^n{}_c = \Delta\omega_{n-1}[m\overline{\omega}({r^2}_s - {r^2}_e)] - \Delta\theta^*{}_n[mg\sin\theta^*(r_e - r_s)]. \tag{14}$$

From the approximation in Eq. (9), $\Delta\theta^*{}_n$ can be represented as follows

$$\Delta\theta^*{}_n = -\Delta\omega_{n-1} t^* - \Delta T_{n-1}\overline{\omega}. \tag{15}$$

Substituting Eq. (15) into Eq. (14), we can obtain $\Delta E^n{}_c$ as follows

$$\begin{aligned} \Delta E^n{}_c = {} & \Delta\omega_{n-1}[mg\sin\theta^*(r_e - r_s)t^* + m\overline{\omega}({r^2}_s - {r^2}_e)] \\ & + \Delta T_{n-1}[mg\sin\theta^*\overline{\omega}(r_e - r_s)]. \end{aligned} \tag{16}$$

It is indicated from Eq. (16) that the disturbance of ω and T will result in the disturbance of the complementary energy E_c. Substituting Eq. (2) into Eq. (6) and perturbing ω, we obtain

$$\begin{cases} E^n{}_c = \dfrac{1}{2\cos^2\varphi_0} m {\omega^+{}_n}^2 {r_s}^2 - \dfrac{1}{2} m {\omega^+{}_{n-1}}^2 {r_s}^2 \\ E^n{}_c + \Delta E^n{}_c = \dfrac{1}{2\cos^2\varphi_0} m(\omega^+{}_n + \Delta\omega_n)^2 {r_s}^2 \\ \quad -\frac{1}{2} m(\omega^+{}_{n-1} + \Delta\omega_{n-1})^2 {r_s}^2. \end{cases} \tag{17}$$

Then neglecting the second-order items of $\Delta\omega_{n-1}$, $\Delta\omega_n$ and using the approximation Eq. (9), we obtain

$$\Delta\omega_n = \cos^2\varphi_0\left(\Delta\omega_{n-1} + \frac{\Delta {E^n}_c}{m\overline{\omega}{r_s}^2}\right). \tag{18}$$

Substituting Eq. (16) into Eq. (18), we obtain

$$\begin{cases} \Delta\omega_n = A\Delta\omega_{n-1} + B\Delta T_{n-1} \\ A = \dfrac{\cos^2\varphi_0}{\overline{\omega}{r_s}^2}[g\sin\theta^*(r_e - r_s)t^* - \overline{\omega}({r_e}^2 - {r_s}^2) + \overline{\omega}{r_s}^2] \\ B = \dfrac{\cos^2\varphi_0}{{r_s}^2}[g\sin\theta^*(r_e - r_s)]. \end{cases} \tag{19}$$

According to the approximation Eq. (9), we obtain the relationship between ΔT_{n-1} and ΔT_n as follows:

$$\Delta T_n - \Delta T_{n-1} = \frac{\varphi_0}{\overline{\omega}} - \frac{\varphi_0}{\overline{\omega} + \Delta\omega_{n-1}} \tag{20}$$

neglecting the high-order items of $\Delta\omega_{n-1}$, we obtain

$$\begin{cases} \Delta T_n = C\Delta\omega_{n-1} + D\Delta T_{n-1} \\ C = \dfrac{\varphi_0}{\overline{\omega}^2} \\ D = 1. \end{cases} \tag{21}$$

For the stable gait, it is required that $|\lambda| < 1$. The eigenvalues could have imaginary parts, as was the case for passive model, but in the model with trajectory control they have no imaginary [17]. So the following inequation should be satisfied

$$A - 1 < BC < 0. \tag{22}$$

We will prove that $A - 1 < BC$ is always satisfied as will be stated next. It is obversely that $\varphi_0 < \frac{\pi}{2}$ and $\theta^* < \frac{\pi}{4}$, therefore we obtain the following inequations

$$\begin{cases} \dfrac{\overline{\omega}}{2}\left(t^* - \dfrac{\varphi_0}{\overline{\omega}}\right) \le \dfrac{\varphi_0}{2} < 1 \\ \sin\theta^* < \cos\theta^*. \end{cases} \tag{23}$$

Then if $\dot{r} > 0$, we obtain the following inequation:

$$mg\sin\theta^*(r_e - r_s)\frac{\overline{\omega}}{2}\left(t^* - \frac{\varphi_0}{\overline{\omega}}\right) < mg\cos\theta^*(r_e - r_s). \tag{24}$$

Combing Eqs. (2), (5), (7) and (13), we obtain the following equation

$$mg\cos\theta^*(r_e - r_s) = \frac{1}{2}m\overline{\omega}^2{r_s}^2\tan^2\varphi_0 + \frac{1}{2}m\overline{\omega}^2({r_e}^2 - {r_s}^2). \tag{25}$$

Substituting Eq. (25) into Eq. (24), we obtain the following inequation

$$g\sin\theta^*(r_e - r_s)(t^* - \frac{\varphi_0}{\overline{\omega}}) - \overline{\omega}({r_e}^2 - {r_s}^2) < \overline{\omega}{r_s}^2\tan^2\varphi_0. \tag{26}$$

Then Eq. (26) can be rewritten as follows

$$\frac{\cos^2\varphi_0}{\overline{\omega}{r_s}^2}[g\sin\theta^*(r_e - r_s)t^* - \overline{\omega}({r_e}^2 - {r_s}^2) + \overline{\omega}{r_s}^2] - 1 < \frac{\cos^2\varphi_0}{{r_s}^2}g\sin\theta^*(r_e - r_s)\cdot\frac{\varphi_0}{\overline{\omega}^2}. \tag{27}$$

Therefore, $A-1 < BC$ is always satisfied. Since $C > 0$, it is required that $B < 0$ and $\dot{r} > 0$ for the Eq. (22) to be satisfied. From $B < 0$, we can obtain that

$$\sin\theta^* < 0 \quad (\dot{r} > 0). \tag{28}$$

Since $\theta_s < \theta^* < \theta_e$, Eq. (28) can be fully satisfied by $\theta_s \le 0$ & $\theta_e < 0$. Finally, basic Condition II for the stable gait is as follows

$$\theta_s \le 0 \quad \& \quad \theta_e < 0 \quad (\dot{r} > 0). \tag{29}$$

Eq. (29) means that the timing of extending the stance leg should be after the midpoint in the swing phase.

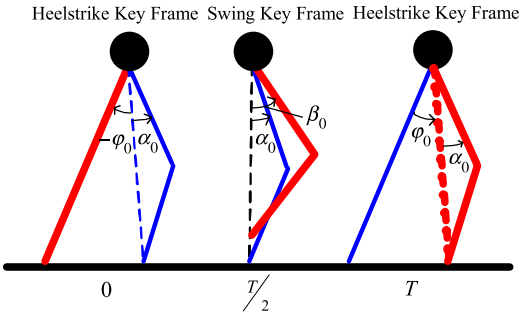

Fig. 9. Sagittal movement.

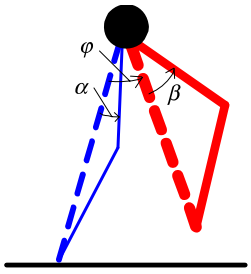

Fig. 10. Definition of key frame parameters.

4. Gait generation

The implementation of forward walking is applying Virtual Slope Walking in the sagittal plane with the Lateral Swing Movement for lateral stability. The sideward walking and turning is realized by carefully designing the key frames. All of the above gait is generated by connecting the key frames with smooth sinusoids.

4.1. Forward walking

We divide the forward walking into two separate motions in orthogonal planes called the sagittal and lateral plane. Virtual Slope Walking is realized in the sagittal plane while Lateral Swing Movement is in the lateral plane to avoid falling sideward.

4.1.1. Virtual Slope Walking in the sagittal plane

The gait generation begins with the creation of swing and stance leg trajectories based on the principle of Virtual Slope Walking. According to the basic conditions of Virtual Slope Walking, the energy conservation equation is correlated with the state of heelstrike. Also, the stance leg should be extended after the midpoint in the swing phase. Consequently, the stance leg trajectory can be generated by connecting three key frames as one step: Heelstrike and Swing frame as shown in Fig. 9. The Heelstrike Key Frame is set at the moment of just after heelstrike as the start of one step, which is also the end of one step for the periodic repetition of the gait. The Swing Key Frame is set at the midpoint of the swing phase. The swing leg is controlled to the correct pose for the Heelstrike Key Frame without contacting the ground. For the symmetric in the forward walking, two steps make a stride.

These three key frames are parameterized by four parameters as shown in Fig. 9. The definition of the parameters with the positive sign is shown in Fig. 10. We first define the virtual leg as the line joining the hip point and the end of the actual leg. φ is the angle from the virtual stance leg to the virtual swing leg with the initial value φ_0 determining the step length. α is the angle from the virtual stance leg to the thigh, determining the stance leg length. The initial value α_0 is related to the amount of the complementary energy E_c, the larger α_0 is, the more energy is added. β is the angle

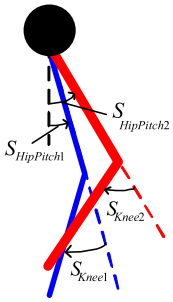

Fig. 11. Definition of joint angles in sagittal plane.

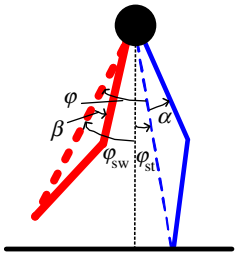

Fig. 12. Transformation from φ to hip angles.

from the virtual swing leg to the thigh, determining the swing leg length. β_0 is related to the lifting height of the swing leg at the midpoint of the swing phase. T is the step period. According to the Eq. (7), a higher step frequency (small T) resulting in higher angular velocity ω or a larger step length (large φ_0) will dissipate more energy during heelstrike. So the faster the robot walks, the larger α_0 should be.

Since the exact shape of the trajectories for the joints are of little concern in Virtual Slope Walking, we simply use smooth sinusoids to connect these three key frames as described by Eq. (30).

$$\begin{cases} \varphi = -\varphi_0 \cos\dfrac{\pi t}{T} \\ \alpha = \alpha_0 \\ \beta = -\dfrac{\beta_0}{2}\cos\dfrac{2\pi t}{T} + \dfrac{\beta_0}{2} \\ 0 < t \le \dfrac{T}{2} \end{cases} \quad \begin{cases} \varphi = -\varphi_0 \cos\dfrac{\pi t}{T} \\ \alpha = -\dfrac{\alpha_0}{2}\cos\dfrac{2\pi t}{T} + \dfrac{\alpha_0}{2} \\ \beta = -\dfrac{\beta_0 - \alpha_0}{2}\cos\dfrac{2\pi t}{T} + \dfrac{\beta_0 + \alpha_0}{2} \\ \dfrac{T}{2} < t \le T. \end{cases} \tag{30}$$

In practical walking, it is required to transform the trajectories of φ, α and β to the trajectories of the joint angles. The definition of the joint angles with the positive sign is shown in Fig. 11. φ is divided into φ_{st} and φ_{sw} to control the upper body to be upright during walking, as shown in Fig. 12.

Therefore, the hip angles can be represented as follows

$$\begin{aligned} S_{HipPitch1} &= \alpha + \varphi_{st} \\ S_{HipPitch2} &= \beta + \varphi_{sw} \\ \varphi_{st} &= \begin{cases} \dfrac{(\varphi_0 - \varphi_1)}{2}\cos\dfrac{2\pi t}{T} + \dfrac{(\varphi_0 - \varphi_1)}{2} & 0 < t \le \dfrac{T}{2} \\ -\dfrac{\varphi_1}{2}\cos\dfrac{2\pi t}{T} - \dfrac{\varphi_1}{2} & \dfrac{T}{2} < t \le T \end{cases} \\ \varphi_{sw} &= \begin{cases} -\dfrac{\varphi_1}{2}\cos\dfrac{2\pi t}{T} - \dfrac{\varphi_1}{2} & 0 < t \le \dfrac{T}{2} \\ \dfrac{(\varphi_0 - \varphi_1)}{2}\cos\dfrac{2\pi t}{T} + \dfrac{(\varphi_0 - \varphi_1)}{2} & \dfrac{T}{2} < t \le T \end{cases} \\ \varphi_1 &= |\varphi_{sw}(t=0)| = \arctan\frac{1 - \cos\alpha_0 \cos\varphi_0}{\cos\alpha_0 \sin\varphi_0}. \end{aligned} \tag{31}$$

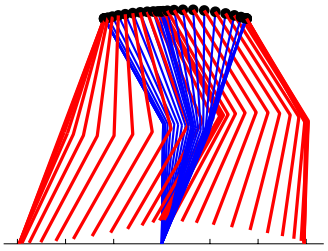

Fig. 13. Stick diagrams for $T = 0.3$ s, $\varphi_0 = 35°$, $\alpha_0 = 15°$, $\beta_0 = 30°$.

The knee angles can be represented as follows

$$\begin{aligned} S_{Knee1} &= 2\alpha \\ S_{Knee2} &= 2\beta. \end{aligned} \tag{32}$$

Therefore, combing Eqs. (30)–(32), The trajectories of the joint angles can be represented as follows

$$\begin{cases} S_{HipPitch1} = \dfrac{(\varphi_0 - \varphi_1)}{2}\left(1 + \cos\dfrac{2\pi t}{T}\right) + \alpha_0 \\ S_{HipPitch2} = -\dfrac{\varphi_1}{2}\left(1 + \cos\dfrac{2\pi t}{T}\right) \\ \quad + \frac{\beta_0}{2}\left(1 - \cos\frac{2\pi t}{T}\right) \\ S_{Knee1} = 2\alpha_0 \\ S_{Knee2} = \beta_0\left(1 - \cos\dfrac{2\pi t}{T}\right) \end{cases} \quad 0 < t \le \frac{T}{2}$$

$$\begin{cases} S_{HipPitch1} = -\dfrac{\varphi_1}{2}\left(1 + \cos\dfrac{2\pi t}{T}\right) + \dfrac{\alpha_0}{2}\left(1 - \cos\dfrac{2\pi t}{T}\right) \\ S_{HipPitch2} = \dfrac{(\varphi_0 - \varphi_1)}{2}\left(1 + \cos\dfrac{2\pi t}{T}\right) \\ \quad + \frac{\alpha_0 + \beta_0}{2} + \frac{\alpha_0 - \beta_0}{2}\cos\frac{2\pi t}{T} \\ S_{Knee1} = \alpha_0\left(1 - \cos\dfrac{2\pi t}{T}\right) \\ S_{Knee2} = 2\alpha_0 + (\beta_0 - \alpha_0)\left(1 - \cos\dfrac{2\pi t}{T}\right) \end{cases} \quad \frac{T}{2} < t \le T \tag{33}$$

$$\varphi_1 = \arctan\frac{1 - \cos\alpha_0 \cos\varphi_0}{\cos\alpha_0 \sin\varphi_0}.$$

The walking motion defined in Eq. (33) is shown in Fig. 13 using a stick diagram.

This gait can easily satisfy the two basic conditions described in Section 3. Tuning the parameter of α_0 will result in the change of the complementary energy E_c. Therefore, Condition I can be satisfied by adjusting the complementary energy E_c to the dissipation energy E_r in the parameters tuning experiment.

According to the trajectory defined in Eq. (33), from $t = 0$ to $t = \frac{T}{2}$, the angle of the stance leg knee joint is a constant, meaning that the leg length is a constant, i.e. $\dot{r} = 0$. From $t = \frac{T}{2}$ to $t = T$, the angle of the stance leg knee joint decreases from $2\alpha_0$ to α_0, meaning that the leg length is increasing, i.e. $\dot{r} > 0$. So the timing of the stance leg extending is after the midpoint o f the swing phase. Therefore, Condition II is satisfied.

4.1.2. Lateral swing movement in the lateral plane

The lateral motion should produce consistent and stable oscillations while keeping the feet flat on the ground. During steady forward walking, the average lateral velocity of the body should be zero and expected to change sign once. We use five key frames to produce such rolling motion for one walking stride as shown in Fig. 14, which is named Lateral Swing Movement. In the key frames of Lateral Swing Movement, γ_0 indicates the lateral swing amplitude. ψ_0 indicates the angle between the two legs and in part determines the lateral swing period [18].

The Lateral Swing Movement will affect the sagittal movement by influencing the position and timing of the heelstrike. By adjusting ψ_0 and γ_0, the lateral and sagittal movement could be

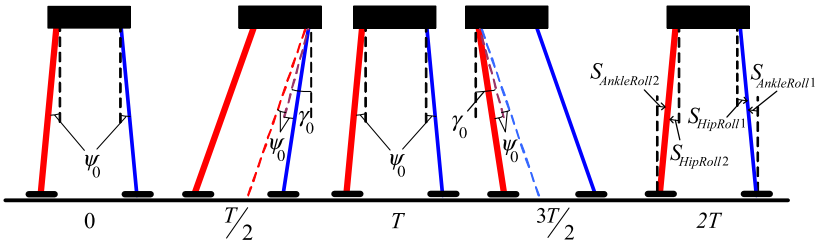

Fig. 14. Lateral Swing Movement and definition of joint angles.

synchronized, which avoids the robot falling sideward. The ankle roll joints are controlled to be parallel to the ground. These five key frames are connected by sinusoids as defined in Eq. (34). The definition of the lateral joint angles with the positive sign is shown in Fig. 14.

$$\begin{aligned} S_{HipRoll1} &= S_{AnkleRoll1} = \psi_0 - \gamma_0 \sin\frac{\pi t}{T} \\ S_{HipRoll2} &= S_{AnkleRoll2} = \psi_0 + \gamma_0 \sin\frac{\pi t}{T}. \end{aligned} \tag{34}$$

4.2. Sideward walking

Sideward walking is composed of both Lateral Swing Movement (Fig. 14) and Lateral Step Movement (Fig. 15). Lateral Step Movement includes three key frames, as shown in Fig. 15. In the key frames of Lateral Step Movement, $2\phi_0$ indicates the lateral step length. The ankle roll joints are controlled to be parallel to the ground. The key frames are connected by sinusoids as defined in Eq. (35).

$$\begin{aligned} S_{HipRoll1} &= S_{AnkleRoll1} = \psi_0 - \gamma_0 \sin\frac{\pi t}{T} + \phi_0 \cos\frac{\pi t}{T} \\ S_{HipRoll2} &= S_{AnkleRoll2} = \psi_0 + \gamma_0 \sin\frac{\pi t}{T} + \phi_0 \cos\frac{\pi t}{T}. \end{aligned} \tag{35}$$

4.3. Turning

For the rotational movement in the transverse plane, three key frames are defined as shown in Fig. 16. λ_0 indicates the rotation amplitude. The key frames are connected by sinusoids as defined in Eq. (36). The definition of the joint angles with the positive sign is shown in Fig. 16.

$$R_{HipYaw1} = R_{HipYaw2} = \lambda_0 \cos\frac{\pi t}{T}. \tag{36}$$

4.4. Omnidirectional walking

By amalgamating the translational movements with the rotational movements, Stepper-3D is able to perform omnidirectional walking. Walking in the sagittal and transverse plane simultaneously, the robot could approach the ball and turn to the goal at the same time. Also, the lateral and rotational movement generate the motion named turn with ball which is quite useful in the kicking adjustment.

5. Experimental results

5.1. Virtual Slope Walking in Stepper-2D

According to the model of Virtual Slope Walking presented in Section 3, we first test the gait in Stepper-2D, which is a planar biped robot mounted on a boom to constrain the body motion in the sagittal plane shown in Fig. 17. Stepper-2D is 368 mm in height and 780 g in weight. And the leg with the point foot is

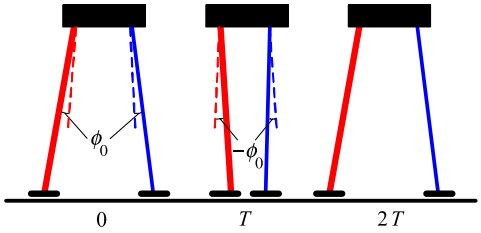

Fig. 15. Lateral Step Movement.

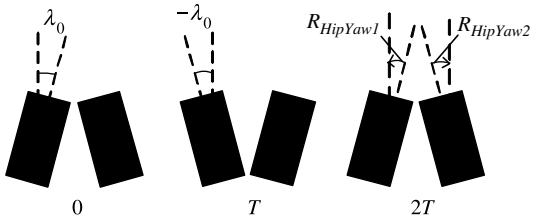

Fig. 16. Rotational movement and definition of joint angles.

Fig. 17. Stepper-2D.

actuated in the hip and knee joint by the same digital servo motors used in Stepper-3D. The configuration of Stepper-2D is close to the point mass model described in Section 3. Based on the sagittal plane gait described in Section 4.1, Stepper-2D achieves a relative speed of 4.48 leg/s, which is the fastest relative speed among the known planar biped robot. All the videos about the walking experiments of Stepper-2D could be found on our website http://www.au.tsinghua.edu.cn/robotlab/rwg/Robots/Stepper_2D.htm

5.2. Virtual Slope Walking in Stepper-3D

For the application of the soccer robot, the point feet are replaced by flat feet in the leg design of Stepper-3D. The flat feet create the possibility for the robot to perform 3D walking and special motions including kicking and getting up, which are all required in the soccer game. According to the model of Virtual Slope Walking described in Section 3, the torque between the stance leg and the ground during the swing phase should be zero, meaning the stance leg acts as an passive inverted pendulum. We use the PDCM to add the mechanical constraint flat feet to the ankle

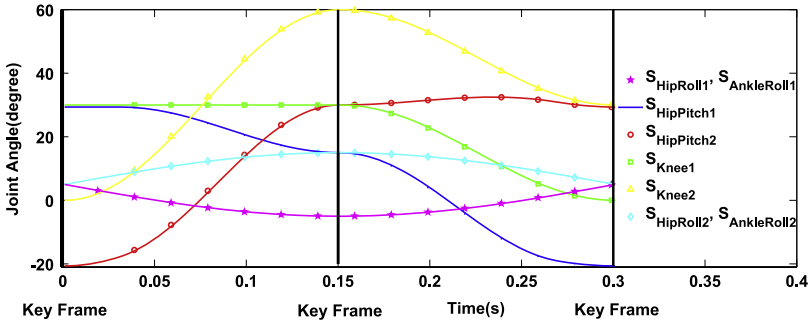

Fig. 18. Trajectories of forward walking joint angles in one walking step. $T = 0.3$ s, $\varphi_0 = 35°$, $\alpha_0 = 15°$, $\beta_0 = 30°$, $\psi_0 = 5°$, $\gamma_0 = 10°$.

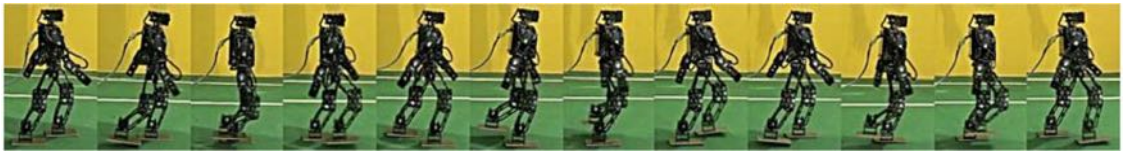

Fig. 19. Forward walking image sequence.

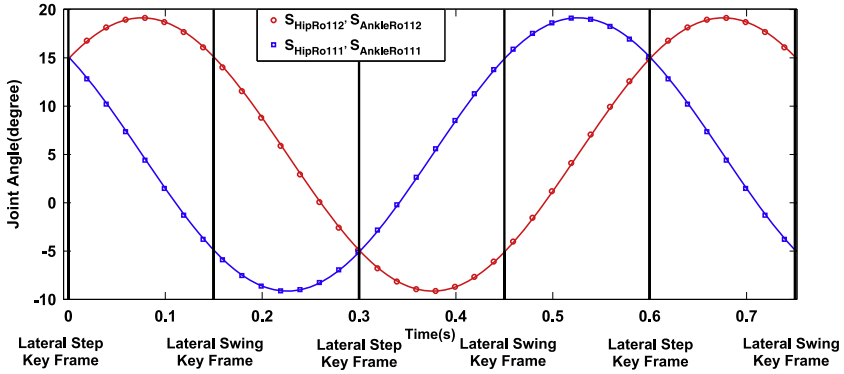

Fig. 20. Trajectories of sideward walking joint angles in 2.5 walking steps. $T = 0.3$ s, $\phi_0 = 10°$, $\gamma_0 = 10°$, $\psi_0 = 5°$.

joint with no actuation. However, the movements of the knee and hip pitch joint will add an additional torque on the ankle pitch joint for the mechanical constraint. Experiment results show that Stepper-3D also achieves a fast walking speed by applying Virtual Slope Walking, which is the same as the result of Stepper-2D. It is indicated that the fast walking comes from the interaction of Virtual Slope Walking and PDCM leg structure. Further explanation will be our further work.

5.2.1. Forward walking

The initial parameters are determined in the simulation by applying Newton-Raphson gradient-based search algorithm. We use the simulation results as the initial parameters for the walking experiment. According to the four parameters of the sagittal movement φ_0, α_0,β_0,T (Fig. 9), the parameter T and φ_0 is related with the walking speed. T should be adapted to the hardware of the robot. Once T is determined, φ_0 can be tuned to produce different walking speed. For a given set of T and φ_0, α_0 determines the falling direction. If the robot falls forward, meaning the complementary energy E_c more than normal, α_0 should be decreased. On the other hand, if the robot falls backward, α_0 should be increased. β_0 is tuned with parameters of the lateral swing movement ψ_0,γ_0 (Fig. 14). The heelstrike position is determined by β_0 and γ_0 while the timing is influenced by ψ_0. Tuning the intuitive and simple parameters with the strategy described above, Stepper-3D reached the speed of 0.5 m/s with the trajectories shown in Fig. 18. By giving different φ_0 and α_0, the robot could change its speed continuously from 0 m/s to 0.5 m/s.

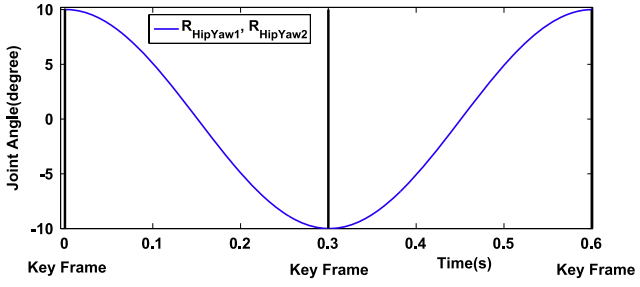

Fig. 21. Trajectories of Rotation Joint Angles in 2 Walking Steps. $T = 0.3$ s, $\lambda_0 = 10°$.

The image sequences of forward walking with the speed of 0.5m/s are shown in Fig. 19.

5.2.2. Sideward walking and turning

By setting $\varphi_0 = 0, \alpha_0 = 0$, tuning β_0 (Fig. 9) and ψ_0, γ_0 (Fig. 14), the robot could march in place. Then by giving a slight value to the lateral step parameter ϕ_0 (Fig. 15) or rotation parameter λ_0 (Fig. 16), it could walk sideward or rotate with the trajectories shown in Figs. 20 and 21 respectively.

The image sequences of sideward walking and turning are shown in Figs. 22 and 23 respectively.

5.2.3. Omnidirectional walking

Omnidirectional walking can be realized by adding the rotational movement to the forward walking or sideward walking.

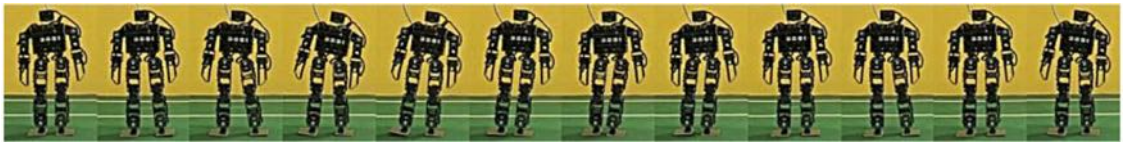

Fig. 22. Sideward walking image sequence.

Fig. 23. Turning image sequence.

In this way, Stepper-3D accomplished walking and rotating simultaneously. All the videos about the walking experiments could be found on our website http://www.au.tsinghua.edu.cn/robotlab/rwg/robots/stepper-3d.htm

6. Conclusion and future work

In this paper, we present the hardware design and gait generation of our humanoid soccer robot Stepper-3D. The parallel double crank mechanism is adopted for the leg structure. The gait is extraordinarily simple with strongly intuitive parameters, which results in a very fast walking speed and also accomplishes omnidirectional walking favorably. Stepper-3D performed fast and stable walking in RoboCup 2008 humanoid kid size competitions. The experimental results from Stepper-2D and Stepper-3D indicate that the hardware design and Virtual Slope Walking are suitable for a fast biped walking robot. The improvement of walking ability will result in the progress of the soccer robot research closer to the ultimate goal of the RoboCup.

The effect of the PDCM on Virtual Slope Walking is one of our future research areas. We can conclude that the PDCM does increase the stability of Virtual Slope Walking from the experiment results. The mechanical constraint flat foot gains stability but maybe loses passiveness. There is a trade-off between the energy efficiency and walking stability. Although we use passive dynamic walking as a starting point, our main interest is in full powered robot with fast and stable walking ability in the dynamic environment. Finding the relationship of the energy supplementation, walking stability and walking speed is the long term goal of this research.

As an application in the soccer robot, we are also working on the modeling of lateral motion in 3D walking to study the stability of the coupled sagittal and lateral movement. What we have achieved in this paper is realizing a 3D walking gait, the theoretical analyze of the lateral stability is needed in the future work. Additionally, according to the intuitive meaning of the Virtual Slope Walking gait parameters, the gait can be optimized by the machine learning approach for speed and environmental adaptability, which is significative in the soccer robot competitions.

Acknowledgements

The authors would like to thank the Tsinghua Hephaestus team. This work was supported partially by the National Natural Science Foundation of China (No. 60875065) and Open Project Foundation of National Robotics Technology and System Key Lab of China (No. SKLRS200718).

References

[1] H. Kitano, M. Asada, The RoboCup Humanoid Challenge as the millennium challenge for advanced robotics, Advanced Robotics 13 (8) (2000) 723–737.
[2] S. Behnke, Online trajectory generation for omnidirectional biped walking, in: Proc. IEEE International Conference on Robotics and Automation, 15–19 May 2006, pp. 1597–1603.
[3] N. Yamato, Y. Akazawa, H. Ishiguro, T. Takahashi, T. Maeda, T. Imagawa, H. Takayama, N. Mitsunaga, T. Miyashita, VisiON NEXTA: Fully autonomous humanoid robot, in: RoboCup 2005 Humanoid League Team Descriptions, Osaka, Japan, 2005.
[4] M. Friedmann, J. Kiener, S. Petters, D. Thomas, O. von Stryk, H. Sakamoto, Versatile, high-quality motions and behavior control of humanoid soccer robots, in: Proc. Workshop on Humanoid Soccer Robots of the 2006 IEEE-RAS Int. Conf. on Humanoid Robots, Genoa, Italy, 4–6 December 2006, pp. 9–16.
[5] Changjiu Zhou, Pik Kong Yue, Robo-Erectus: A low-cost autonomous humanoid soccer robot, Advanced Robotics 18 (7) (2004) 717–720.
[6] M. Vukobratovic, B. Borovac, Zero-moment point thirty five years of its life, International Journal of Humanoid Robotics 1 (1) (2004) 157–173.
[7] M. Hirose, Y. Haikawa, T. Takenaka, et al. Development of humanoid robot ASIMO, in: Proc. IEEE/RSJ International Conference on Intelligent Robots and Systems, Workshop 2, Maui, HI, USA, 29 Oct 2001.
[8] D.G.E. Hobbelen, M. Wisse, Humanoid robots: Human-like machines, Chapter 14: Limit Cycle Walking, I-Tech Education and Publishing, Vienna, Austria, June 2007, p. 642.
[9] S. Collins, A. Ruina, R. Tedrake, et al., Efficient Bipedal Passive-Dynamic Walkers, Science 307 (5712) (2005) 1082–1085.
[10] T. McGeer, Passive Dynamic Walking, International Journal of Robotics Research 9 (1990) 62–82.
[11] T. McGeer, Stability and control of two-dimensional biped walking. Technical Report CSS-IS TR 88-01, Simon Fraser University, 1988.
[12] M. Wisse, Three additions to passive dynamic walking; actuation, an upper body, and 3d stability, in: Proc., Int. Conf. on Humanoid Robots, IEEE, Los Angeles, USA, 2004.
[13] D.G.E. Hobbelen, M. Wisse, Ankle Actuation for Limit Cycle Walkers, International Journal of Robotics Research 27 (6) (2008) 709–735.
[14] S.H Collins, A.A. Ruina, Bipedal walking robot with efficient and human-like gait, in: Proc. IEEE International Conference on Robotics and Automation, 18–22 April 2005, pp. 1983–1988.
[15] P. Kulvanit, O. Stryk, RoboCup Soccer Humanoid League Rules and Setup for the 2008 competition in Suzhou, China, https://lists.cc.gatech.edu/mailman/listinfo/robocup-humanoid.
[16] M. Wisse, Essentials of dynamic walking: Analysis and design of two-legged robots. Ph.D. Thesis, Delft University of Technology, Netherlands, 2004.
[17] M. Wisse, C.G. Atkeson, D.K. Kloimwieder, Swing leg retraction helps biped walking stability, in: IEEE-RAS International Conference on Humanoid Robots, 5 Dec. 2005, pp. 295–300.
[18] M. Garcia, Stability, scaling, and chaos in passive dynamic gait models. Ph.D. Thesis, Cornell University, Ithaca, NY, 1999.

H. Dong is a Ph.D. candidate in Robotics and Intelligent Control Lab, Department of Automation, Tsinghua University. He was born in Inner Mongolia, China, in 1984. He received the ME Bachelor Degree in Department of Precision Instruments and Mechanology of Tsinghua University in 2004. Currently, he is working on the stability analysis of Virtual Slope Walking.

M.G. Zhao is an Associate Professor of Department of Automation, Tsinghua University. He received his BE, MS and PhD degree from Harbin Institute of Technology in 1995, 1997 and 2001 respectively. From 2001 to 2003, he got a post doctor position in Department of Precision Instrument, Tsinghua University. His research interest includes Biped Locomotion Control and Robot Self-Localization.

J. Zhang was born in a small town called Tanggu on the east coast of China, Mainland in 1984. He received his Bachelor Degree of Engineering in Department of Automation, Tsinghua University in 2008. His work covers Four-legged Walking, CPG driven Biped, and currently a new method that he brought forward-Virtual Slope Walking for Biped Robot. His work mainly focuses on the walking stability and energetics analsis.

Prof. N.Y. Zhang graduated from the Department of Electrical Engineering of Tsinghua University in 1970. Since then, he has been engaged in the teaching and research work in the Department of Automation, Tsinghua University. He has been in Stuttgart University, Germany as a visiting scholar from 1992 to 1993. His current research interests include: hierarchical fuzzy systems and control, intelligent control of robot soccer, etc.